



Extended Kalman Filtering and Nonlinear Predictive Filtering for Spacecraft Attitude Determination

A.H.J. de Ruiter * C.J. Damaren *

ABSTRACT

Demands in the design and manufacture of spacecraft are changing. Smaller, lower cost spacecraft are becoming increasingly more desirable, while the required spacecraft performance is increasing (consider the space telescope, which is required to accurately track a star). Use of cheaper hardware would lower the spacecraft performance, but this effect may be offset by the use of more sophisticated controller and estimation schemes. This paper compares the Extended Kalman Filter (which has traditionally been used for spacecraft attitude determination) with a relatively new filter, the Nonlinear Predictive Filter. It is shown that under certain circumstances the Nonlinear Predictive Filter outperforms the Extended Kalman Filter, but that the requirements for these circumstances (namely, the use of rate sensors) conflict with the robustness requirement with respect to initial estimate error.

continued on page 14

1. INTRODUCTION

There is a trend towards building smaller, lower cost spacecraft, which use cheaper, lower quality hardware. At the same time, the required spacecraft performance is increasing (consider the space telescope, which is required to accurately track a star). The decrease in performance due to the use of cheaper hardware may be offset via the use of more sophisticated controller and estimation schemes.

Traditionally, the Extended Kalman Filter (EKF) has been used for spacecraft attitude determination. This has the advantage that it is computationally inexpensive, and fairly robust with respect to model errors. However, it has the disadvantage that it is a linearized technique, and this suggests that the region of stability is small, since non-linearities in the plant dynamics are not fully accounted for.

A recent addition to the family of non-linear filters is the Nonlinear Predictive Filter (NPF). The NPF was derived by Crassidis and Markley (1997a). This filter has the advantage that no assumption is made about the magnitude or form of the model error. In fact, the model error is "found" as part of the filtering procedure. The NPF is also computationally inexpensive to implement.

This paper presents the numerical application of both the EKF and the NPF to the spacecraft attitude determination problem. Crassidis and Markley (1997b) have also applied the NPF to the spacecraft attitude determination problem. However, they do not compare it with the EKF, and the spacecraft dynamics are formulated differently. Crassidis and Markley use the angular momentum and quaternions as the states, this paper uses the angular velocity and Euler angles. In practice, quaternions are preferred from the singularity avoidance point of view, but for simplicity we use Euler angles since the trajectory in question avoids the singularity anyway.

In this paper, two scenarios are considered. In the first, angular rate measurements, magnetometer measurements, and Sun-sensor measurements are all available. In the second, all but the rate sensors are available. The filter performance measure is the root mean square of the rate and orientation errors, and the filter performances are compared with respect to plant error, measurement error, initial estimate error, and sensor noise level.

* Institute for Aerospace Studies
University of Toronto
4925 Dufferin Street
Toronto, ON M3H 5T6, Canada

Received 12 February 2002.



suite de la page 13

RÉSUMÉ

Les exigences en matière de conception et de fabrication des engins spatiaux sont en pleine effervescence. Il est de plus en plus préférable de construire des petits engins spatiaux peu coûteux et très performants (pensez seulement au télescope spatial qui doit poursuivre les étoiles avec précision). L'utilisation de matériaux moins coûteux réduirait le rendement de l'engin spatial, mais cet effet peut être contré en ayant recours à de meilleures techniques de commande de l'appareil et d'évaluation des coûts du projet. Ce mémoire compare le filtre de Kalman étendu (qui était traditionnellement utilisé pour déterminer l'attitude d'un engin spatial) à un filtre relativement nouveau, le filtre prédictif non linéaire. Il est démontré que dans certaines conditions, le filtre prédictif non linéaire est plus performant que le filtre de Kalman étendu. Certaines de ces conditions (notamment l'utilisation de détecteurs de vitesse) sont incompatibles avec les exigences portant sur la robustesse de l'appareil par rapport à l'estimation initiale des probabilités d'erreur.

2. FILTER ALGORITHMS

2.1 The Extended Kalman Filter

Since the EKF is well-known, and has been in use for a long time, the algorithm is not summarized here. A full derivation of the EKF is given by Jazwinski (1970).

2.2 The Nonlinear Predictive Filter

The full derivation of the NPF is presented by Crassidis and Markley (1997a). The algorithm for its implementation is given here.

In the NPF, the state estimates are obtained by propagating an equation of the plant dynamics, which are assumed to be of the form

$$\dot{\hat{\mathbf{x}}} = \mathbf{f}(\hat{\mathbf{x}}) + \mathbf{G}(\hat{\mathbf{x}})\mathbf{d}(t_k), \quad t_k \leq t \leq t_{k+1} \quad (1)$$

where $\mathbf{d}(t_k)$ is a to be determined model error vector. The output estimate is given by

$$\hat{\mathbf{y}} = \mathbf{h}(\hat{\mathbf{x}}) \quad (2)$$

State observable discrete measurements are assumed to be of the following form:

$$\mathbf{y}_k = \mathbf{h}(\mathbf{x}_k) + \mathbf{v}_k \quad (3)$$

where \mathbf{v}_k is a zero-mean, Gaussian white-noise process with

$$E\{\mathbf{v}_k\} = 0$$

$$E\{\mathbf{v}_k \mathbf{v}_l^T\} = \mathbf{R} \delta_{kl}$$

where $E\{\cdot\}$ denotes the expectation operator.

Expanding the output estimate Equation (2) in a Taylor series from one sampling instant to the next gives

$$\hat{\mathbf{y}}(t_{k+1}) = \hat{\mathbf{y}}(t_k) + \mathbf{z}(\hat{\mathbf{x}}(t_k), \Delta t) + \mathbf{\Lambda}(\Delta t) \mathbf{S}(\hat{\mathbf{x}}(t_k)) \mathbf{d}(t_k) \quad (4)$$

where Δt is the sampling period and

$$\mathbf{z}(\hat{\mathbf{x}}(t_k), \Delta t) = \text{col} \left\{ \sum_{k=1}^{p_i} \frac{\Delta t^k}{k!} L_f^k(h_i) \right\} \quad (5)$$

$$\mathbf{\Lambda}(\Delta t) = \text{diag} \left\{ \frac{\Delta t^{p_i}}{p_i!} \right\} \quad (6)$$

$$\mathbf{S}(\hat{\mathbf{x}}(t_k)) = \text{col} \left\{ L_{g_i} [L_f^{p_i-1}(h_i)] \right\} \quad (7)$$

and p_i is the lowest order of the derivatives of $h_i(\hat{\mathbf{x}}(t_k))$ in which any component of $\mathbf{d}(t_k)$ appears.

$L_f^k(h_i)$ is a k th-order Lie derivative and is given by

$$L_f^0(h_i) = h_i$$

$$L_f^k(h_i) = \frac{\partial L_f^{k-1}(h_i)}{\partial \hat{\mathbf{x}}^T} \mathbf{f}(\hat{\mathbf{x}}, t_k), \quad k \geq 1$$

The Lie derivative with respect to L_{g_i} is given by

$$L_{g_i} [L_f^{p_i-1}(h_i)] = \frac{\partial L_f^{p_i-1}(h_i)}{\partial \hat{\mathbf{x}}^T} \mathbf{G}(\hat{\mathbf{x}}, t_k)$$

The model error vector $\mathbf{d}(t_k)$ is found at each sampling instant to minimize the cost functional

$$J(\mathbf{d}(t_k)) = \frac{1}{2} [\mathbf{y}(t_{k+1}) - \hat{\mathbf{y}}(t_{k+1})]^T \mathbf{R}^{-1} [\mathbf{y}(t_{k+1}) - \hat{\mathbf{y}}(t_{k+1})] + \frac{1}{2} \mathbf{d}(t_k)^T \mathbf{W} \mathbf{d}(t_k) \quad (8)$$

where $\mathbf{W} \in \mathbf{R}^{q \times q}$ is a positive semi-definite weighting matrix.

Substituting Equation (4) into Equation (8) and minimizing gives the model error $\mathbf{d}(t_k)$

$$\begin{aligned} \mathbf{d}(t_k) = & -\{\mathbf{S}(\hat{\mathbf{x}}(t_k))^T \mathbf{\Lambda}(\Delta t)^T \mathbf{R}^{-1} \mathbf{\Lambda}(\Delta t) \mathbf{S}(\hat{\mathbf{x}}(t_k)) \\ & + \mathbf{W}\}^{-1} \mathbf{S}(\hat{\mathbf{x}}(t_k))^T \mathbf{\Lambda}(\Delta t)^T \mathbf{R}^{-1} \\ & \times [\mathbf{z}(\hat{\mathbf{x}}(t_k), \Delta t) - \mathbf{y}(t_{k+1}) + \hat{\mathbf{y}}(t_k)] \end{aligned} \quad (9)$$

The NPF algorithm can then be found using the following steps.

1. Calculate $\mathbf{\Lambda}(\Delta t)$ from Equation (6).



2. Store $\hat{\mathbf{x}}(t_k)$, $\hat{\mathbf{y}}(t_k)$, and $\mathbf{y}(t_{k+1})$.
3. Calculate $\mathbf{z}(\hat{\mathbf{x}}(t_k), t_k)$ and $\mathbf{S}(\hat{\mathbf{x}}(t_k))$ from Equations (5) and (7), respectively.
4. Calculate $\mathbf{d}(t_k)$ from Equation (9).
5. Integrate Equation (1) from t_k to t_{k+1} to get $\hat{\mathbf{x}}(t_{k+1})$ and $\hat{\mathbf{y}}(t_{k+1})$.
6. Set k to $k + 1$.
7. Return to 2.

3. SPACECRAFT ATTITUDE DYNAMICS

The spacecraft is assumed to be in a Keplerian orbit. The spacecraft motion equation is given by

$$\mathbf{I}\dot{\boldsymbol{\omega}} + \boldsymbol{\omega} \times \mathbf{I}\boldsymbol{\omega} = \mathbf{G}_g + \mathbf{G}_m + \mathbf{G}_a + \mathbf{G}_s \quad (10)$$

where \mathbf{I} is the spacecraft inertia matrix and $\boldsymbol{\omega}$ is the absolute angular velocity of the spacecraft.

\mathbf{G}_g , \mathbf{G}_m , \mathbf{G}_a , and \mathbf{G}_s are the gravity-gradient, geomagnetic, aerodynamic, and solar pressure torques, respectively. They are given by

$$\mathbf{G}_g = \frac{3\mu}{r^5} \mathbf{R}_b \times \mathbf{I} \mathbf{R}_b \quad (11)$$

$$\mathbf{G}_m = \mathbf{m}_b \times \mathbf{B}_b \quad (12)$$

$$\mathbf{G}_a = \mathbf{c}_{pa} \times \mathbf{F}_a \quad (13)$$

$$\mathbf{G}_s = \mathbf{c}_{ps} \times \mathbf{F}_s \quad (14)$$

where \mathbf{R}_b , \mathbf{m}_b , and \mathbf{B}_b are the spacecraft position, spacecraft residual magnetic dipole moment, and Earth's magnetic field, respectively, expressed in the spacecraft frame of reference. The vectors \mathbf{c}_{pa} and \mathbf{c}_{ps} are the spacecraft centers of pressure corresponding to the aerodynamic pressure and the solar pressure, respectively. The vectors \mathbf{F}_a and \mathbf{F}_s are the net aerodynamic and solar pressure forces on the spacecraft, respectively, μ is the geocentric gravitational constant and $r = |\mathbf{R}_b|$.

The geomagnetic field model is the dipole approximation given by Wertz (1985). In inertial coordinates, the geomagnetic field is given by

$$\mathbf{B}_I = \begin{bmatrix} (B_r \cos \delta + B_\theta \sin \delta) \cos \alpha - B_\phi \sin \alpha \\ (B_r \cos \delta + B_\theta \sin \delta) \sin \alpha - B_\phi \cos \alpha \\ B_r \sin \delta - B_\theta \cos \delta \end{bmatrix}$$

where α and δ are the spacecraft right ascension and declination, respectively. The geomagnetic field components in spherical coordinates are given by

$$B_r = 2 \left(\frac{a_e}{r} \right)^3 [g_1^0 \cos \theta_m + (g_1^1 \cos \phi_m + h_1^1 \sin \phi_m) \sin \theta_m]$$

$$B_\theta = \left(\frac{a_e}{r} \right)^3 [g_1^0 \sin \theta_m - (g_1^1 \cos \phi_m + h_1^1 \sin \phi_m) \cos \theta_m]$$

$$B_\phi = \left(\frac{a_e}{r} \right)^3 [g_1^1 \sin \phi_m - h_1^1 \cos \phi_m]$$

where θ_m and ϕ_m are the co-elevation and east-longitude of the spacecraft, a_e is the radius of the Earth, and g_1^0 , g_1^1 , and h_1^1 are geomagnetic field coefficients.

The spacecraft attitude is parameterized by a 3–2–1 Euler sequence, $\boldsymbol{\theta} = [\theta_1 \theta_2 \theta_3]^T$. The corresponding attitude kinematics are given by

$$\dot{\boldsymbol{\theta}} = \mathbf{S}^{-1}(\boldsymbol{\theta}) \boldsymbol{\omega} \quad (15)$$

where

$$\mathbf{S}^{-1}(\boldsymbol{\theta}) = \begin{bmatrix} 1 & \sin \theta_1 \tan \theta_2 & \cos \theta_1 \tan \theta_2 \\ 0 & \cos \theta_1 & -\sin \theta_1 \\ 0 & \sin \theta_1 \sec \theta_2 & \cos \theta_1 \sec \theta_2 \end{bmatrix}$$

Defining the state vector to consist of the angular velocity and attitude parameterization, $\mathbf{x}^T \triangleq [\boldsymbol{\omega}^T \boldsymbol{\theta}^T]$, the attitude dynamics are given in first-order form by

$$\dot{\mathbf{x}} = \mathbf{f}(\mathbf{x}, t) \quad (16)$$

where

$$\mathbf{f}(\mathbf{x}, t) = \begin{bmatrix} \mathbf{I}^{-1}(-\boldsymbol{\omega} \times \mathbf{I}\boldsymbol{\omega} + \mathbf{G}_g + \mathbf{G}_m + \mathbf{G}_a + \mathbf{G}_s) \\ \mathbf{S}^{-1}(\boldsymbol{\theta}) \boldsymbol{\omega} \end{bmatrix}$$

The filters are given no knowledge of the geomagnetic-, aerodynamic-, and solar-pressure torques; hence these are treated as disturbance torques. Thus, the nominal plant used for filter design is given by

$$\dot{\mathbf{x}} = \hat{\mathbf{f}}(\mathbf{x}, t) \quad (17)$$

with

$$\hat{\mathbf{f}}(\mathbf{x}, t) = \begin{bmatrix} \mathbf{I}^{-1}(-\boldsymbol{\omega} \times \mathbf{I}\boldsymbol{\omega} + \mathbf{G}_g) \\ \mathbf{S}^{-1}(\boldsymbol{\theta}) \boldsymbol{\omega} \end{bmatrix}$$

Note that the spacecraft is controls free. The justification for this is that the controls are additive to the dynamics equations, and their inclusion in the filter designs would also be additive.



Since in both the plant and filter equations they depend on the state estimates, they cancel out in the error dynamics.

4. MEASUREMENT EQUATIONS

In the first scenario, measurements of the angular rate, Earth's magnetic field, and the Sun position vector are available. The measurement equation for this case is given by

$$y_k = \begin{bmatrix} \boldsymbol{\omega}(t_k) \\ \mathbf{C}_{\text{bl}}(\boldsymbol{\theta}(t_k))\mathbf{B}_I \\ \mathbf{C}_{\text{bl}}(\boldsymbol{\theta}(t_k))\mathbf{s}_I \end{bmatrix} + \begin{bmatrix} \mathbf{v}_{\omega k} \\ \mathbf{v}_{mk} \\ \mathbf{v}_{sk} \end{bmatrix} \quad (18)$$

where \mathbf{C}_{bl} is the rotation matrix from inertial to spacecraft coordinates corresponding to $\boldsymbol{\theta}$. The vectors \mathbf{B}_I and \mathbf{s}_I are the Earth's magnetic field and Sun-pointing vector given in inertial coordinates. The vectors $\mathbf{v}_{\omega k}$, \mathbf{v}_{mk} and \mathbf{v}_{sk} are additive noises with discrete-time covariances

$$E\{\mathbf{v}_{\omega k}\mathbf{v}_{\omega l}^T\} = r_{\omega}\mathbf{1}\delta_{kl}$$

$$E\{\mathbf{v}_{mk}\mathbf{v}_{ml}^T\} = r_m\mathbf{1}\delta_{kl}$$

$$E\{\mathbf{v}_{sk}\mathbf{v}_{sl}^T\} = r_s\mathbf{1}\delta_{kl}$$

The Sun measurements are not available during the time when the spacecraft is in eclipse, and are removed at that time.

In the second scenario, the rate measurements are removed, and it is assumed that the Sun measurements are available at all times (i.e., no eclipse). The measurement equation in this case is given by

$$y_k = \begin{bmatrix} \mathbf{C}_{\text{bl}}(\boldsymbol{\theta}(t_k))\mathbf{B}_I \\ \mathbf{C}_{\text{bl}}(\boldsymbol{\theta}(t_k))\mathbf{s}_I \end{bmatrix} + \begin{bmatrix} \mathbf{v}_{mk} \\ \mathbf{v}_{sk} \end{bmatrix} \quad (19)$$

5. PREDICTIVE FILTER COMPONENTS

The equation for the attitude kinematics, Equation (15), is exact, and hence the model error need only be added to the spacecraft dynamics equation ($\mathbf{d}(t_k) \in \mathbf{R}^3$). In the first scenario it is added as a disturbance torque, and in this case the filter equation becomes

$$\dot{\hat{\mathbf{x}}} = \hat{\mathbf{f}}(\hat{\mathbf{x}}, t) + \mathbf{G}\mathbf{d}(t_k) \quad (20)$$

where

$$\mathbf{G} = \begin{bmatrix} \mathbf{I}^{-1} \\ \mathbf{0} \end{bmatrix} \quad (21)$$

In the second scenario (no rate sensor), the model error is added directly to the filter dynamics, and hence in this case

$$\mathbf{G} = \begin{bmatrix} \mathbf{1} \\ \mathbf{0} \end{bmatrix} \quad (22)$$

5.1 Angular Rate Measurements

The angular rate measurement depends directly on $\boldsymbol{\omega}$, and hence, the order of p_i in this case is 1. Hence,

$$z_{\omega} = (\Delta t)L_f^1(h_{\omega})$$

$$\Lambda(\Delta t)_{\omega} = (\Delta t)\mathbf{1}$$

5.2 Magnetometer and Sun-Sensor Measurements

The magnetometer and Sun-sensor measurements do not depend explicitly on $\boldsymbol{\omega}$, and hence, the lowest order of derivative of those in which any component of $\mathbf{d}(t_k)$ appears is $p_i = 2$. Thus,

$$z_m = (\Delta t)L_f^1(h_m) + \frac{(\Delta t)^2}{2}L_f^2(h_m)$$

$$\Lambda(\Delta t)_m = \frac{(\Delta t)^2}{2}\mathbf{1}$$

and

$$z_s = (\Delta t)L_f^1(h_s) + \frac{(\Delta t)^2}{2}L_f^2(h_s)$$

$$\Lambda(\Delta t)_s = \frac{(\Delta t)^2}{2}\mathbf{1}$$

In scenario 1,

$$\mathbf{z} = \begin{bmatrix} z_{\omega} \\ z_m \\ z_s \end{bmatrix}, \quad \Lambda = \begin{bmatrix} \Lambda_{\omega} & 0 & 0 \\ 0 & \Lambda_m & 0 \\ 0 & 0 & \Lambda_s \end{bmatrix}$$

In scenario 2,

$$\mathbf{z} = \begin{bmatrix} z_m \\ z_s \end{bmatrix}, \quad \Lambda = \begin{bmatrix} \Lambda_m & 0 \\ 0 & \Lambda_s \end{bmatrix}$$

5.3 Lie Derivatives

The first-order Lie derivatives are given by

$$L_f^1(h_{\omega}) = \mathbf{I}^{-1}[-\boldsymbol{\omega}^{\times}\mathbf{I}\boldsymbol{\omega} + \mathbf{G}_g]$$

$$L_f^1(h_m) = \frac{\partial(\mathbf{C}_{\text{bl}}(\hat{\boldsymbol{\theta}})\mathbf{B}_I)}{\partial\hat{\boldsymbol{\theta}}^T} \mathbf{S}^{-1}(\hat{\boldsymbol{\theta}})\boldsymbol{\omega}$$

$$L_f^1(h_s) = \frac{\partial(\mathbf{C}_{\text{bl}}(\hat{\boldsymbol{\theta}})\mathbf{s}_I)}{\partial\hat{\boldsymbol{\theta}}^T} \mathbf{S}^{-1}(\hat{\boldsymbol{\theta}})\boldsymbol{\omega}$$



The second-order Lie derivatives are given by

$$L_f^2(h_m) = \frac{\partial(C_{bl}(\hat{\theta})B_l)}{\partial\hat{\theta}^T} S^{-1}(\hat{\theta})I^{-1}[-\omega \times I\omega + G_g] \\ + \frac{\partial}{\partial\hat{\theta}^T} \left[\frac{\partial(C_{bl}(\hat{\theta})B_l)}{\partial\hat{\theta}^T} S^{-1}(\hat{\theta})\omega \right] S^{-1}(\hat{\theta})\omega$$

$$L_f^2(h_s) = \frac{\partial(C_{bl}(\hat{\theta})s_l)}{\partial\hat{\theta}^T} S^{-1}(\hat{\theta})I^{-1}[-\omega \times I\omega + G_g] \\ + \frac{\partial}{\partial\hat{\theta}^T} \left[\frac{\partial(C_{bl}(\hat{\theta})s_l)}{\partial\hat{\theta}^T} S^{-1}(\hat{\theta})\omega \right] S^{-1}(\hat{\theta})\omega$$

The Lie derivatives with respect to L_{g_i} in scenario 1 are given by

$$L_{g\omega}[L_f^0(h_\omega)] = I^{-1}$$

$$L_{gm}[L_f^1(h_m)] = \frac{\partial(C_{bl}(\hat{\theta})B_l)}{\partial\hat{\theta}^T} S^{-1}(\hat{\theta})I^{-1}$$

$$L_{gs}[L_f^1(h_s)] = \frac{\partial(C_{bl}(\hat{\theta})s_l)}{\partial\hat{\theta}^T} S^{-1}(\hat{\theta})I^{-1}$$

and in scenario 2,

$$L_{gm}[L_f^1(h_m)] = \frac{\partial(C_{bl}(\hat{\theta})B_l)}{\partial\hat{\theta}^T} S^{-1}(\hat{\theta})$$

$$L_{gs}[L_f^1(h_s)] = \frac{\partial(C_{bl}(\hat{\theta})s_l)}{\partial\hat{\theta}^T} S^{-1}(\hat{\theta})$$

6. SIMULATION DESCRIPTIONS

6.1 Orbital Dynamics

The spacecraft orbit is assumed to be Keplerian, and the same for all simulations. The orbital elements are given in **Table 1**.

Table 1. Orbital elements.

a (km)	e	i (deg)	Ω (deg)	ω (deg)	t_0 (s)
7171.2	0	94.6	157.5	180	0

6.2 Magnetic-Field Model

The radius of the Earth is taken to be $a_e = 6371.2$ km. The geomagnetic field constants are: $g_1^0 = -29\,682$ nT, $g_1^1 = -1789$ nT, and $h_1^1 = 5310$ nT.

6.3 Spacecraft Characteristics

The spacecraft inertia matrix is given by $I = \text{diag}\{[10\ 12\ 2]\}$ kg m², and the spacecraft residual magnetic dipole moment is $m_b = [0.1\ 0.1\ 0.1]^T$ A m².

6.4 Numerical Integration and Sampling Rate

The simulation is Fortran based and the spacecraft states are propagated using a fourth-order Runge–Kutta procedure with the stepsize being the sampling period, $T_s = 0.1$ s.

6.5 Spacecraft Initial Conditions

The spacecraft initial conditions are

$$x(0) = [0.005\ \text{rad/s}\ 0.005\ \text{rad/s}\ 0.005\ \text{rad/s}\ 10^\circ\ 10^\circ\ 10^\circ]^T$$

6.6 Sensor Noise and Sensor Suites

The sensor noise components are generated using the equation

$$v_i = \sqrt{12r_i} \left[\sigma_i - \frac{1}{2} \right] \quad (23)$$

where σ_i is a random variable between 0 and 1 generated using the Fortran intrinsic function Rand . The values of the sensor noise covariances are given in **Table 2**.

Table 2. Sensor noise covariance.

$\sqrt{r_\omega}$ (T)	$\sqrt{r_m}$ (deg/s)	$\sqrt{r_s}$ (deg)
0.00016	2×10^{-9}	0.0014

6.7 Performance Measures

The filter performance is measured by calculating the root mean square (rms) of the angular rate and Euler angle errors. These are given by

$$E_{\text{rms}_\omega} = \left\{ \frac{\sum_{k=1}^n e_{\omega k}^T e_{\omega k}}{n} \right\}^{1/2} \quad (24)$$

$$E_{\text{rms}_\theta} = \left\{ \frac{\sum_{k=1}^n e_{\theta k}^T e_{\theta k}}{n} \right\}^{1/2} \quad (25)$$

where $e_{\omega k} = \omega(t_k) - \hat{\omega}(t_k)$ and $e_{\theta k} = \theta(t_k) - \hat{\theta}(t_k)$ are the estimation errors in the angular rates and Euler angles, respectively, and n is the total number of estimate updates during the simulation.

6.8 Plant Error

Model error in the plant is introduced by errors in the spacecraft inertia matrix. The true spacecraft inertia matrix remains fixed throughout all simulations, but the filter knowledge of it changes from simulation to simulation. The error in the inertia matrix is introduced in two ways simultaneously. There is an error in the value of the principal inertias, and there is an offset of the principal axes. The filter principal inertias are calculated from

$$\{I_{pe}\}_{i,i} = \{I_{pt}\}_{i,i}[1 + 0.02e_p], \quad i = 1, 2, 3$$



where $\{I_{pt}\}_{i,i}$ and $\{I_{pe}\}_{i,i}$ are the true and filter principal inertias, respectively. The angular offset of the principal axes is given by a 3–2–1 Euler sequence

$$\boldsymbol{\theta}_1 = e_p [3^\circ \ 3^\circ \ 3^\circ]^T$$

From this the filter inertia matrix is calculated

$$I_e = C^T(\boldsymbol{\theta}_1) I_{pe} C(\boldsymbol{\theta}_1)$$

where $C(\boldsymbol{\theta})$ is the rotation matrix corresponding to $\boldsymbol{\theta}_1$. It is clear then that e_p is a measure of the plant error.

6.9 Measurement Error

Model error in the measurements is introduced in two ways simultaneously. The filter knowledge of the geomagnetic field is not exact, and the sensors are offset. The geomagnetic field (as far as the filter is aware) is calculated using the geomagnetic-field constants given by

$$g_{1e}^0 = g_1^0 (1 + 0.01 e_m)$$

$$g_{1e}^1 = g_1^1 (1 + 0.01 e_m)$$

$$h_{1e}^1 = h_1^1 (1 + 0.01 e_m)$$

The Earth's radius (as far as the filter is aware) is calculated from

$$a_{ee} = a_e (1 + 0.01 e_m)$$

The angular offsets of the sensors are given by 3–2–1 Euler sequences

$$\boldsymbol{\theta}_\omega = e_m [1^\circ \ -1^\circ \ 1^\circ]^T$$

$$\boldsymbol{\theta}_m = e_m [-1^\circ \ 1^\circ \ 1^\circ]^T$$

$$\boldsymbol{\theta}_s = e_m [1^\circ \ 1^\circ \ -1^\circ]^T$$

for the rate-sensor, magnetometer, and Sun-sensor, respectively. Thus, the actual measurements are given by

$$y_k = \begin{bmatrix} C(\boldsymbol{\theta}_\omega) \boldsymbol{\omega}(t_k) \\ C(\boldsymbol{\theta}_m) C_{bi}(\boldsymbol{\theta}(t_k)) \mathbf{B}_1(t_k) \\ C(\boldsymbol{\theta}_s) C_{bi}(\boldsymbol{\theta}(t_k)) s_1(t_k) \end{bmatrix} + \begin{bmatrix} v_{\omega k} \\ v_{mk} \\ v_{sk} \end{bmatrix}$$

where $C(\boldsymbol{\theta}_i)$ is the rotation matrix corresponding to $\boldsymbol{\theta}_i$. Thus, e_m is a measure of the measurement error.

6.10 Initial Estimate Error

The initial condition of the state estimates is given by

$$\hat{\mathbf{x}}(0) = \mathbf{x}(0) + e_i \bar{e}$$

where for scenario 1

$$\bar{e} = [0.005 \text{ rad/s} \ 0.005 \text{ rad/s} \ 0.005 \text{ rad/s} \ 1^\circ \ 1^\circ \ 1^\circ]^T$$

and for scenario 2

$$\bar{e} = [0.005 \text{ rad/s} \ 0.005 \text{ rad/s} \ 0.005 \text{ rad/s} \ 5^\circ \ 5^\circ \ 5^\circ]^T$$

Hence, e_i is a measure of the initial estimate error.

6.11 Filter Tuning

For the EKF, the discrete-time plant noise covariance matrix, \mathbf{Q} is assumed to be of the form

$$\mathbf{Q} = \begin{bmatrix} q\mathbf{1} & \mathbf{0} \\ \mathbf{0} & \mathbf{0} \end{bmatrix}$$

For the NPF, the model error weighting matrix, \mathbf{W} , is assumed to be of the form

$$\mathbf{W} = w\mathbf{1}$$

In tuning the filters, e_p , e_m , and e_i were set to zero (the filter is designed for the nominal plant), and q and w were sought to minimize $E_{\text{rms}\omega}$ and $E_{\text{rms}\theta}$. The minimum for both did not always occur for the same value of q or w , and a compromise was achieved instead.

In scenario 1, the values chosen are, $q = 5 \times 10^{-12} \text{ s}^{-4}$ and $w = 1 \times 10^4 \text{ kg}^2 \text{ m}^4 \text{ s}^{-4}$. In scenario 2 they are $q = 5 \times 10^{-12} \text{ s}^{-4}$ and $w = 5 \times 10^6 \text{ s}^{-4}$.

6.12 Simulations Performed

With the filters tuned for the nominal plant, the filters were perturbed to examine performance with respect to plant error, measurement error, and sensitivity to initial estimate error. The simulation sets are summarized in **Table 3**. Simulation set 1 examines the filter sensitivity to plant error, simulation set 2 examines the filter sensitivity to measurement error, and simulation set 3 examines the filter sensitivity to initial estimate error. All simulation sets were run for both sensor suite scenarios. Simulations were also performed for the nominal plant ($e_p = e_m = e_i = 0$) where the sensor noise levels in **Table 2** were multiplied by 10 and 100. The filters were redesigned for the new sensor noise levels (although this was only necessary for the NPF in scenario 2).

Table 3. Simulation sets.

Simulation set	e_p range	e_m range	e_i range
1	–6, 6	0	0
2	0	–6, 6	0
3	0	0	–6, 6



7. SIMULATION RESULTS

7.1 Plant Error

As shown in **Figures 1 and 2**, the NPF with rate measurements has no sensitivity to plant error. The EKF performance on the other hand, becomes progressively worse as the plant error increases. The EKF Euler angle estimates are affected more by the plant error than the angular rate estimates. This is not surprising given that the angular rates are measured directly whereas the Euler angles are not.

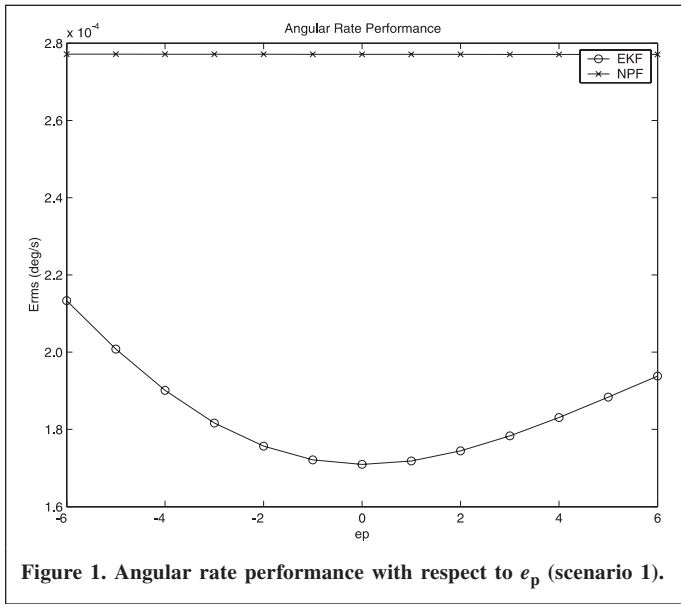


Figure 1. Angular rate performance with respect to e_p (scenario 1).

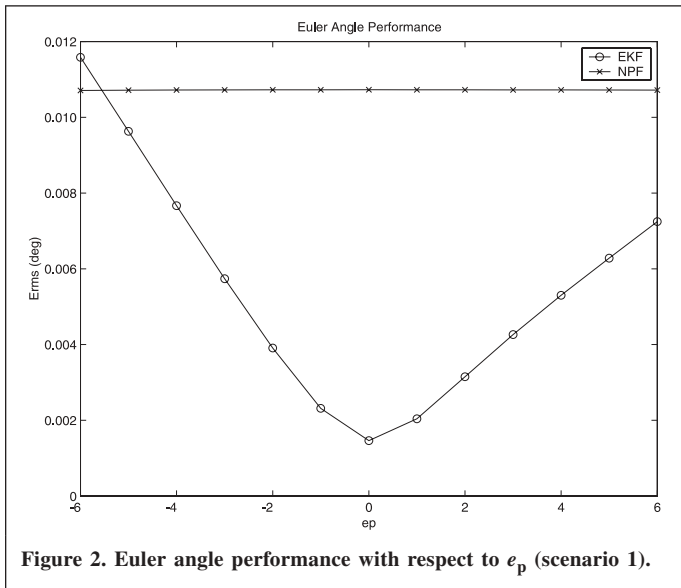


Figure 2. Euler angle performance with respect to e_p (scenario 1).

The situation is reversed for the EKF when the rate measurements are removed (see **Figures 3 and 4**). The angular rate estimates are much more sensitive to plant error, and the Euler angle estimates are less sensitive. As in the case with rate sensors, the NPF angular rate estimates are completely insensitive to plant error, however, the removal of the rate

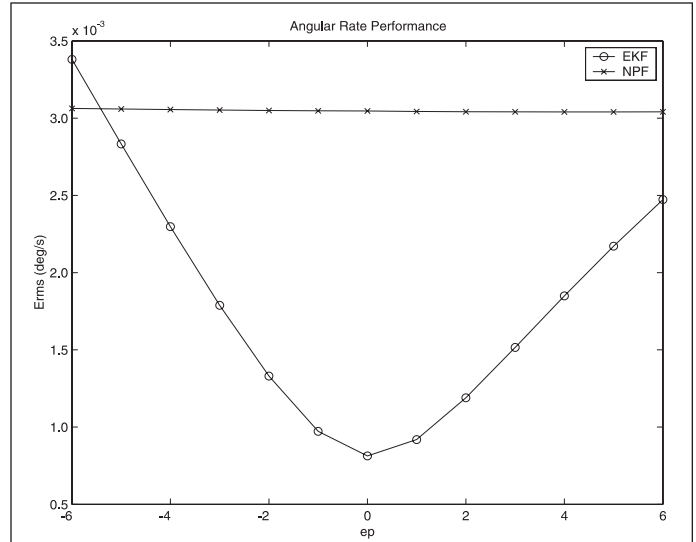


Figure 3. Angular rate performance with respect to e_p (scenario 2).

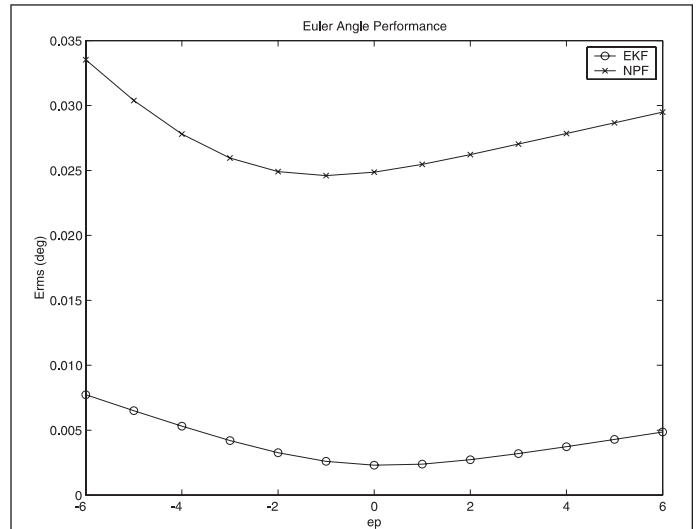


Figure 4. Euler angle performance with respect to e_p (scenario 2).

sensor results in the NPF Euler angle estimates getting worse as the plant error is increased.

Figures 1 and 2 suggest that for large plant errors, the NPF will out-perform the EKF when rate measurements are available. This conclusion cannot be drawn for the case when rate measurements are not available. **Figure 4** shows that the Euler angle estimates become worse at a quicker rate for the NPF than the EKF when the plant error is increased.

The conclusion that can be drawn from these results is that for the most robust estimates with respect to plant error, the NPF should be used with rate sensors present.

7.2 Measurement Error

Figure 5 shows that both the EKF and the NPF angular rate estimates have essentially the same sensitivity to measurement error when rate measurements are available. The EKF fares

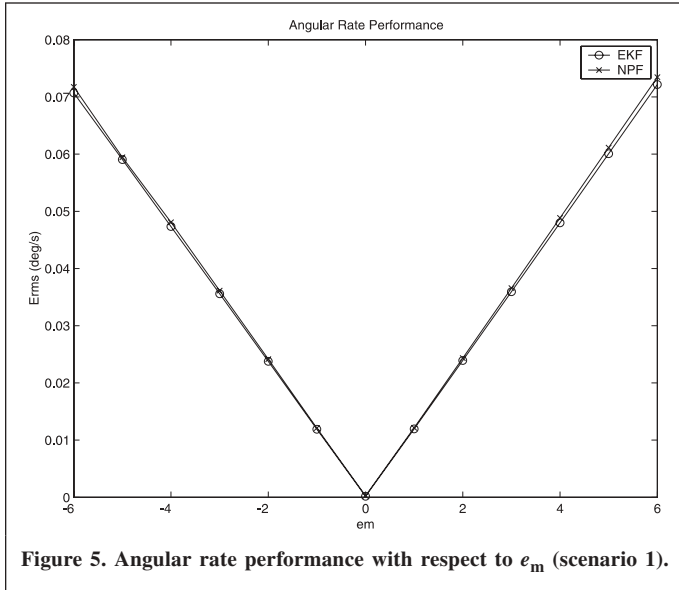


Figure 5. Angular rate performance with respect to e_m (scenario 1).

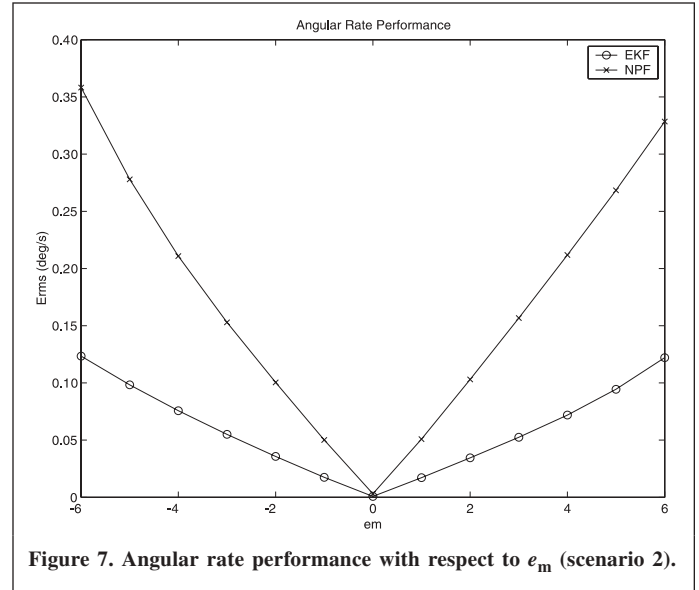


Figure 7. Angular rate performance with respect to e_m (scenario 2).

slightly better, but the difference is not significant. **Figure 6** on the other hand, shows that when rate measurements are available, the NPF performs significantly better than the EKF for Euler angle estimates. The reverse is true when rate measurements are not available. The NPF and EKF performances are almost identical for the Euler angle estimates, but the EKF significantly outperforms the NPF for the angular rate estimates (see **Figures 7** and **8**).

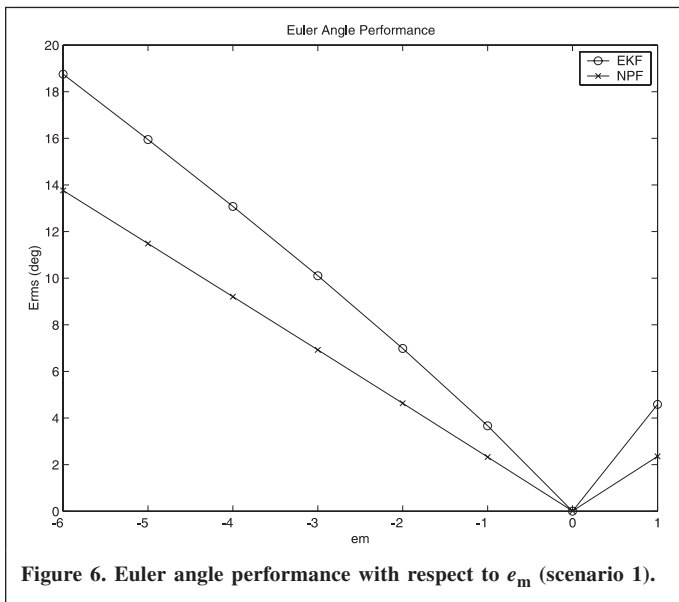


Figure 6. Euler angle performance with respect to e_m (scenario 1).

It is also noteworthy from comparing **Figures 5** and **7**, that the angular rate estimates are significantly worse when the rate measurements are not available. The Euler angle estimates are also worse when the rate measurements are not available.

Comparing **Figures 5**, **6**, **7**, and **8**, it can be concluded that the most robust filter with respect to measurement error is the NPF when the rate measurements are available. The least

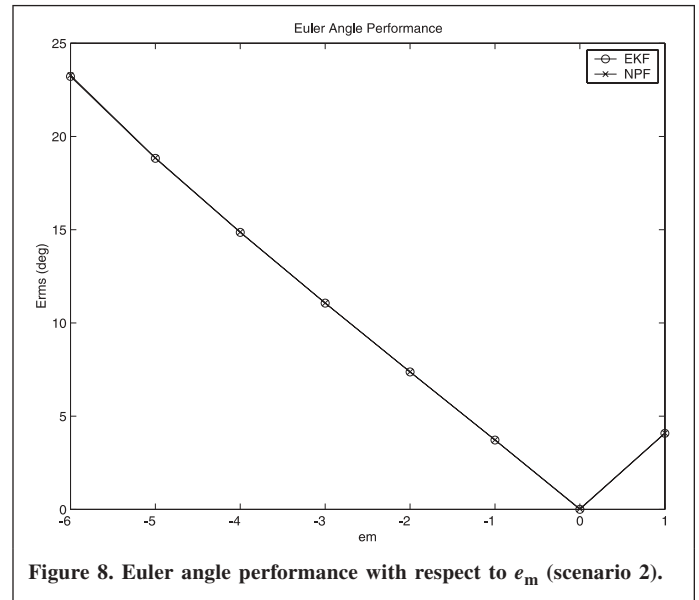


Figure 8. Euler angle performance with respect to e_m (scenario 2).

robust filter with respect to measurement error is the NPF without rate measurements.

7.3 Initial Estimate Error

Figure 9 shows that with rate sensors, the EKF and NPF perform essentially the same for the angular rate estimates with respect to initial condition error. This is not too surprising, since with the rates being measured directly, their estimates can be expected to converge rapidly. **Figure 10**, however, tells a completely different story for the Euler angle estimates.

The NPF Euler angle rms estimation error increases rapidly as the initial estimate error increases. This shows that the convergence of the NPF Euler angle estimates is very slow. The EKF Euler angle estimates converge rapidly. In fact, it was found that for initial estimate errors not much larger than those

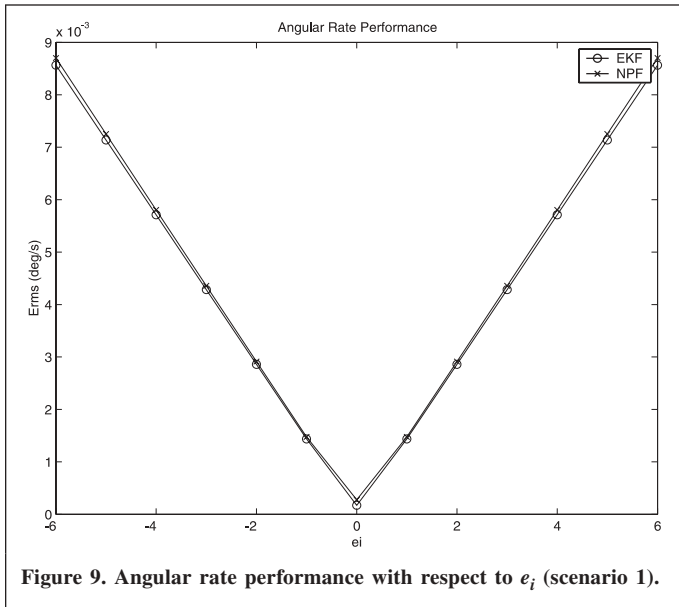


Figure 9. Angular rate performance with respect to e_i (scenario 1).

plotted in **Figure 10**, the NPF did not converge at all in the Euler angles, but did converge in the rates.

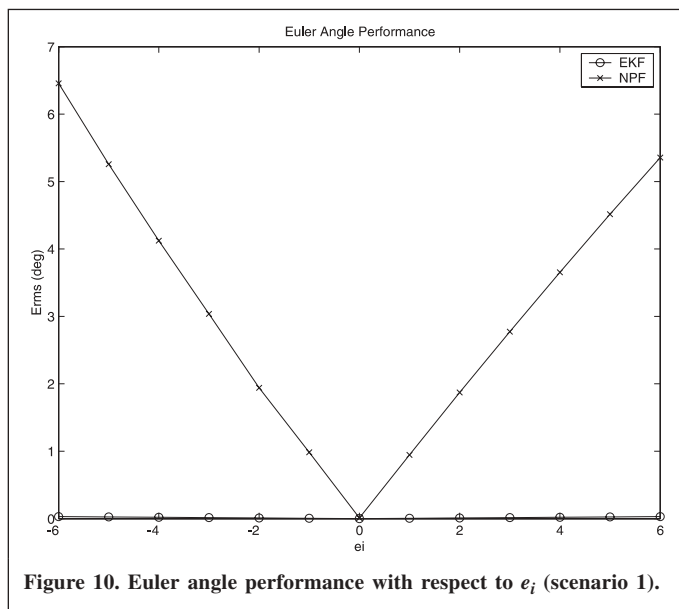


Figure 10. Euler angle performance with respect to e_i (scenario 1).

A possible explanation for this behaviour of the NPF with rate measurements is that unlike the EKF, the Euler angle estimates are not updated directly. They are updated indirectly by integration of Equation (15). The angular rates are however directly updated by the model error, $d(t_k)$. With rate sensors present, the angular rates are included in the cost function of Equation (8), and the filter attempts to track the angular rates at the expense of the Euler angles. Since Euler angles are integrals of the rates, the initial condition of the Euler angles greatly affects the resulting Euler angle trajectory. If the NPF puts most emphasis on tracking the angular rates, then it does not allow the Euler angles to converge.

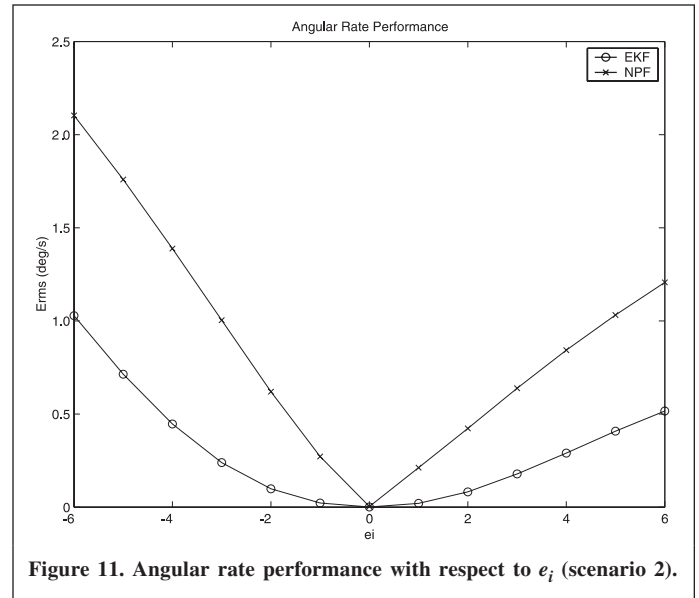


Figure 11. Angular rate performance with respect to e_i (scenario 2).

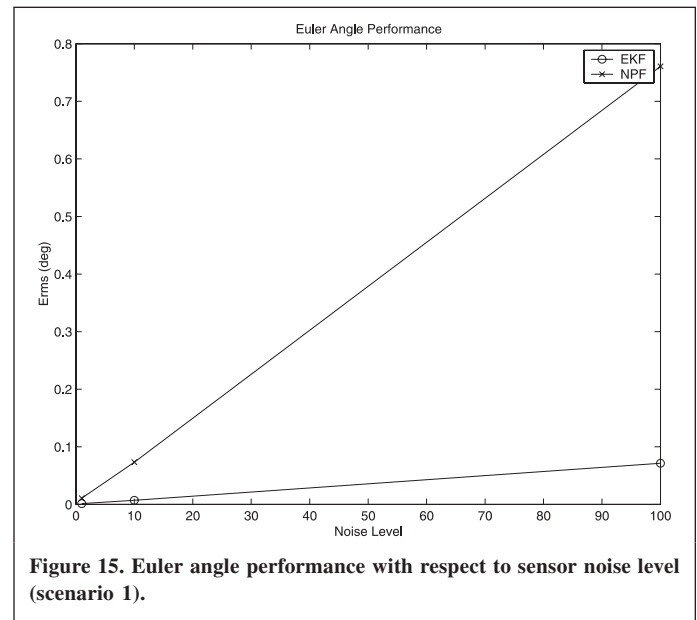
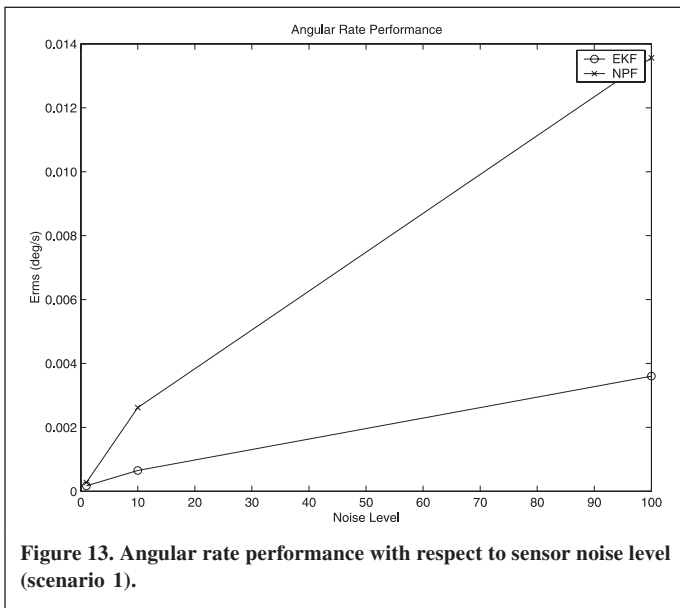
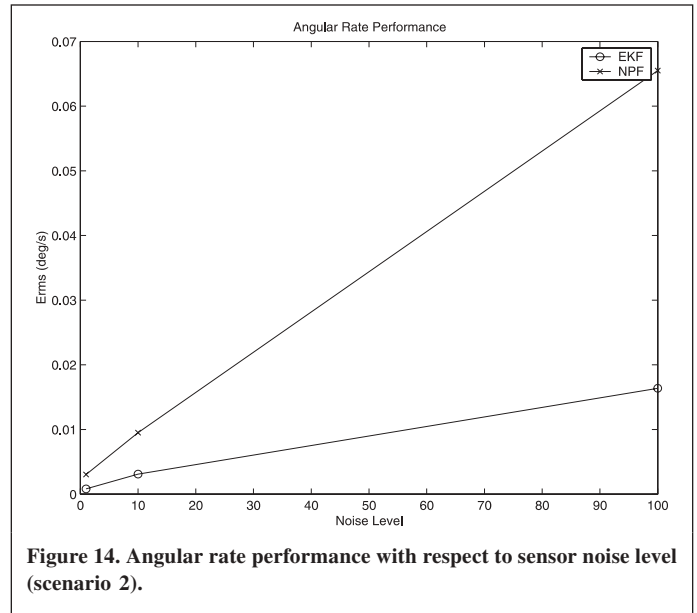
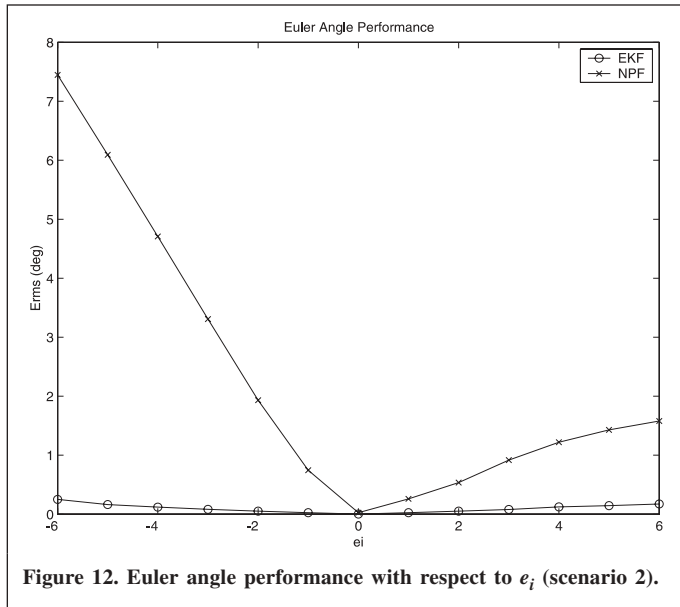
Another point of interest is that with rate measurements available, the EKF was able to converge rapidly for very large initial errors. **Figure 12** seems to confirm the hypothesis outlined above. With the rate sensors removed, the NPF Euler angle estimate performance improved, and was able to be made to converge for much larger initial estimate errors. The cost of this is that the angular rates converge slower. However, this is of little consequence, since if the Euler angles converge, then the rates being derivatives of them must converge also. This does not work in the reverse, it is spoilt by the constant of integration (i.e., initial errors of the Euler angles). In all cases, the EKF converges more quickly than the NPF, but it was found that when the rate sensors were removed, the zone of convergence was larger for the NPF. In summary, the inclusion of rate measurements makes the EKF extremely robust with respect to initial errors, whereas the NPF requires the exclusion of rate measurements to perform acceptably with respect to initial error. In all cases, the EKF exhibits much more rapid convergence (when it does converge) than the NPF.

7.4 Sensitivity to Sensor Noise

Figures 13, 14, 15, and 16 show that the NPF is much more sensitive to sensor noise than the EKF. This can be explained by the fact that the statistics of the sensor noise used in this study match the assumptions used in the design of the EKF whereas the NPF makes no real statistical assumptions on the sensor noise. When the plant is nominal, the EKF is capable of much more accurate state estimates than the NPF.

8. CONCLUDING REMARKS

In this paper we have compared the application of the Extended Kalman Filter and the Nonlinear Projection Filter to the spacecraft attitude determination problem. We have shown that under certain circumstances the Nonlinear Projection Filter outperforms the Extended Kalman Filter, but this requires the



use of rate sensors. This conflicts with the requirement that no rate sensor be used for robustness with respect to initial estimate error.

The results show that the filters are much more sensitive to measurement errors than to plant errors. Hence, in designing a filter for spacecraft attitude determination, much care must be taken to mount the sensors accurately. An accurate model of the spacecraft is less important.

REFERENCES

- Crassidis, J.L., and Markley, F.L. (1997a). "Predictive Filtering for Nonlinear Systems". *J. Guid. Control Dyn.* Vol. 20, pp. 566–572.
- Crassidis, J.L., and Markley, F.L. (1997b). "Predictive Filtering for Attitude Estimation Without Rate Sensors". *J. Guid. Control Dyn.* Vol. 20, pp. 522–527.

Jazwinski, A.H. (1970). "Stochastic Processes and Filtering Theory", Academic Press, London, England.

Wertz, J.R. (1985). "Spacecraft Attitude Determination and Control", D. Reidel Publishing Company, Dordrecht, The Netherlands.

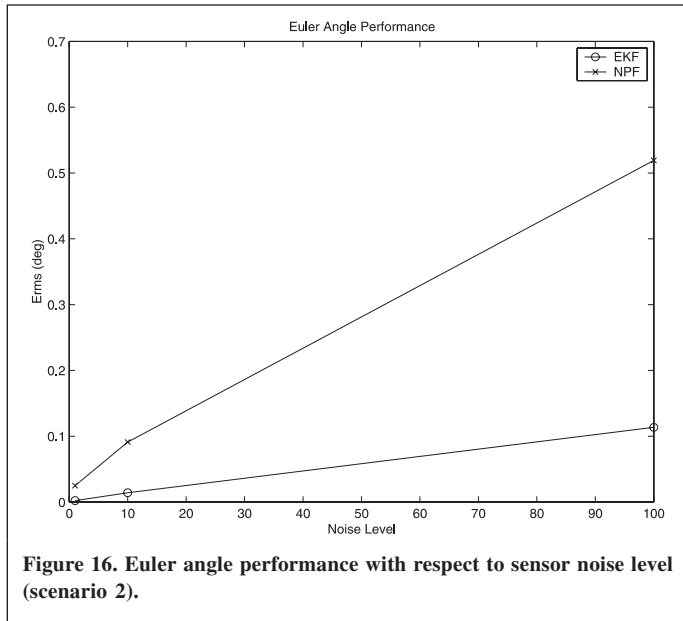


Figure 16. Euler angle performance with respect to sensor noise level (scenario 2).